Invited Paper

A partial-element analysis method for determining resonator coupling in terahertz metamaterials

John F. O'Hara [1*], Patrick L. Colestock [2], and Abul K. Azad [3]
[1] School of Electrical & Computer Engineering, Oklahoma State University
[2] ISR-2, Los Alamos National Laboratory
[3] Center for Integrated Nanotechnologies, Los Alamos National Laboratory
[*1] Email: oharaj@okstate.edu

(Received May 2, 2013)

Abstract: Electric and magnetic coupling mechanisms between resonator elements are increasingly researched as additional tools to be leveraged in engineering the response in terahertz metamaterials. Full-wave simulations can reveal the overall effect of coupling on a metamaterial response but often leave questions about the relative strength of magnetic versus electric effects, and whether one or the other dominates the final response. This letter shows an analytical method called partial-element analysis to estimate and isolate the magnetic and electric interactions in metamaterial unit cells. Several case studies show the utility of the method for predicting resonance shifts in paired split-ring resonators. The extention of partial-element analysis to a more comprehensive simulation technique is briefly discussed and described as an optimistic direction for future analysis and engineering of nonlinear terahertz metamaterials.

Keywords: Metamaterials, Terahertz, Coupling, Magnetic, Electric

doi: 10.11906/TST.095-112.2013.06.06

1. Introduction

Soon after electromagnetic metamaterial research began, it branched into several specialized directions. Some of the higher impact branches included cloaking and transformation optics, optical magnetism, and negative index materials. Research in terahertz metamaterials rapidly gained footing as well, spurred on in large part by original studies of dynamic metamaterials, whose effective constitutive parameters could be actively tuned by some external stimulus [1-3].

Terahertz metamaterial research continues today and now encompasses yet another sub-group of studies involving coupling mechanisms. The term "coupling mechanisms" is actually quite broad and includes many different phenomena observed in experimental and theoretical terahertz metamaterials studies. These include coupling of separate eigenmodes of a single metamaterial resonators [4, 5], coupling of two or more distinct, but neighboring resonators through either electric or magnetic fields [6-9], coupling between distant resonators through radiation [10], coupling of the metamaterial resonator response with some other electromagnetic mode [11, 12], such as an eigenmode of a Fabry-Perot cavity or plasmonic structure, and finally, dynamic

coupling [13, 14]. The motivation for many of these studies has been to introduce new mechanisms by which the macroscopic electromagnetic response of a metamaterial, or more appropriately a metafilm, could be designed. Some examples include increasing the Q-factor of the resonance, enabling resonance splitting, or stabilizing the resonance against fabrication intolerances.

Coupled terahertz metamaterials are often designed from intuitive basic principles. For example, split-ring resonators (SRRs) that are closely spaced should have some amount of magnetic flux linkage, and thereby feature magnetic coupling. Similarly, SRRs with closely-situated gaps should feature strong electric coupling due to the Coulomb interaction between accumulated charges. Determining the exact effects of coupling is generally left to full-wave simulation tools. While very useful, these do not always permit one to distinguish the magnetic and electric effects, or whether one dominates.

In this paper, we show a simple analytical method to estimate coupling effects in terahertz metamaterial resonators. The method borrows from decades-old calculations used in the electromagnetic compatibility arena [15, 16]. Their goal was to accurately determine interference between conductors in integrated-circuit environments without resorting to computationally intensive analytical methods. While today the advent of much more powerful computers has led to the development of comprehensive computational tools, these are still limited in time-domain situations, particularly when nonlinearities are included. To this end, we wish to develop tractable time-domain algorithms with which general circuit configurations may be analyzed. The first step in this process is to consider the coupling mechanisms in detail. We review the basic principles behind resonance coupling, discuss the method, illustrate its utility with some case studies, cover some generalizations to the method, and finally end with a brief discussion.

2. Coupling physics

Understanding coupling in terahertz metamaterials can begin with the familiar lumped-circuit interpretation of metamaterial behavior. This intuitive approach usually employs a resistive-inductive-capacitive (RLC) circuit to describe metamaterials based on the familiar split-ring resonator (SRR) unit cell. This approximation is justified at both the micro- and macroscopic levels. Microscopically, SRRs and other metamaterial resonators have spatial extent on the scale of some fraction of a wavelength, typically around $\lambda/6$. While this isn't small enough to rigorously qualify as 'lumped-element,' it is often a decent approximation. In terahertz work, the metal resonator is too small to contain actual lumped resistors, inductors, or capacitors, so the effective R, L, and C come from the distributed effects of the metal resonator itself. Capacitance C stems predominately from the regions in the SRR in which charge accumulates during oscillation. Inductance L comes from the currents flowing through the resonator during oscillation. An effective resistance R comes from Ohmic losses and radiative effects, the latter being the obvious indicator that the lumped-element approximation is not perfect.

At a macroscopic level, a metafilm usually appears as a resonant effective boundary impedance to the terahertz wave, causing a bandstop response in transmission. The shape of this response is often cleanly Lorentzian, particularly in the fundamental oscillation mode of the resonator. An ideal RLC circuit model has a rigorous Lorentzian form, and can thereby approximate the macroscopic metamaterial resonance. Two transverse electromagnetic (TEM) transmission lines (TL) complete a macroscopic model when the RLC circuit is placed at their junction. This enables the model to account for incident, reflected, and transmitted waves [17]. In this case, the model applies to measurements in which the terahertz is normally incident upon the metamaterial. Continuing this idea, matrix methods may be employed in stratified metamaterial media, where two or more metafilms exist and are spaced by dielectric layers. These enable an accounting for myriad observed terahertz metamaterial behaviors, such as perfect absorption [11] and anti-reflection [12]. The quality of these models is quite remarkable given their great simplicity. They fail, however, when coupling between the separate layers is significant.

Coupling between metamaterial elements can be either electric or magnetic in nature. In this manuscript ‘coupling’ is regarded henceforth as a significant sharing of electric or magnetic energy approximately in the electrostatic limit. This excludes the notion of long-range energy exchange through radiative mechanisms. In the electrostatic limit, consider any two small conducting bodies, or patches, in free space. These will have a mutual geometry-dependent capacitance that links their response through electric interactions. If either patch acquires a non-zero electric charge, it will set up an electric field around it, which the other patch will partially intercept. The greater the interception, the higher the capacitively coupling between two patches. A similar phenomenon is found in magnetic coupling. Consider two fine wire conductors, also called ‘filaments’, situated in free space. These are linked by a geometry-dependent mutual inductance that links their response through magnetic interactions. If either filament acquires a non-zero electric current, it will set up a magnetic field around it, which the other filament will partially intercept. The greater the interception, the higher the inductive coupling between the two filaments. These two very basic principles form the basis of an analytical coupling estimate, which we now present.

3. Elements of partial calculations

Full metamaterial resonators can be built up by combinations of current filaments and small conducting bodies. Filaments are built into larger “bars” and infinitesimal conductors are combined into “patches”. Patches and bars are then combined as the building blocks of the metmaterial resonators. The inductance between bars and capacitance between patches is calculated by the so-called method of “partial coefficients of inductance” and “partial coefficients of potentials”, or partial inductances and partial potentials for short.

3.1 Partial inductance

The partial inductance requires two calculations, the partial self-inductance and the partial mutual-inductance [15]. For the self-inducatance of a bar, refer to Fig. 1. Let $u = l_o / w_o$ and $w=t_o / w_o$, then the restriction $w \leq 0.01$ permits a convenient approximation for the self-inductance

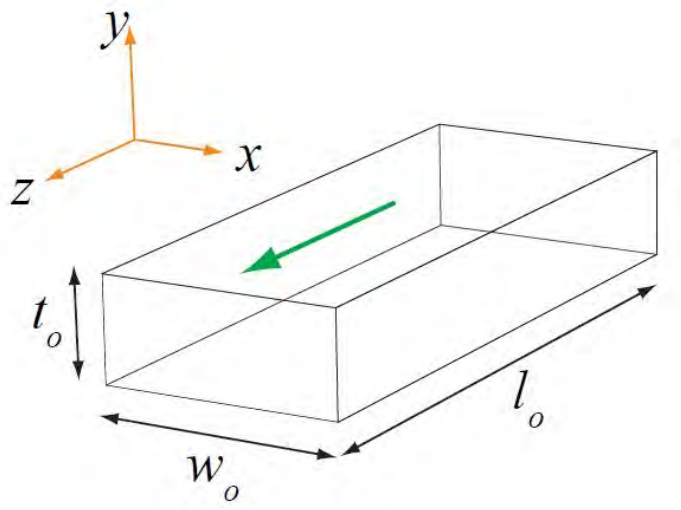

Fig. 1 Layout of integration variables for self partial inductance and mutual partial inductance between two parallel current cells in three dimensions. The green arrows indicate the direction of assumed current flow.

$$Lp_{oo} \approx \frac{\mu_0 l_o}{6\pi}\left\{3\ln\left[u+\sqrt{u^2+1}\right]+u^2+\frac{1}{u}+3u\ln\left[\frac{1}{u}+\sqrt{\frac{1}{u^2}+1}\right]-\frac{1}{u}\left(u^2+1\right)^{\frac{3}{2}}\right\}. \quad (1)$$

where μ_0 is the permeability of free space. For terahertz metamaterials, resonators are often comprised of very thin sheets of metal, and the condition $w \leq 0.01$ is met or nearly met.

Partial mutual inductances between bars of current are calculated somewhat differently. Figure 2 illustrates. The partial mutual inductance is calculated by sub-dividing the bars in the directions transverse to current flow. Each 'sub-bar' is then considered an infinitely thin current filament, for which the mutual inductance is easily calculated. The exact total partial inductance between the bars can be expressed as a limit where bar o is discretized into M parts and bar n is discretized into K parts. As the discretization gets smaller the partial mutual inductance converges, or

$$Lp_{on} = \lim_{\substack{K\to\infty \\ M\to\infty}} \frac{1}{KM}\sum_{k=1}^{K}\sum_{m=1}^{M} Lpf_{mk} \quad (2)$$

where Lpf_{mk} is the partial mutual inductance between any two filaments constituting the bars. Now the filament-to-filament partial inductances are calculated as

$$Lpf_{mk} = \frac{\mu_0 l_o}{4\pi} \sum_{i=1}^{4} (-1)^{i+1} \left\{ g_i \ln \left[g_i + \sqrt{g_i^2 + r^2} \right] - \sqrt{g_i^2 + r^2} \right\} \tag{3}$$

where $r \equiv \sqrt{(\delta x_{km})^2 + (\delta y_{km})^2}/l_o$, $v \equiv l_n/l_o$, $p \equiv \delta_z/l_o$, and

$$g_1 = 1 + p \qquad g_2 = 1 + p - v \qquad g_3 = p - v \qquad g_4 = p,$$

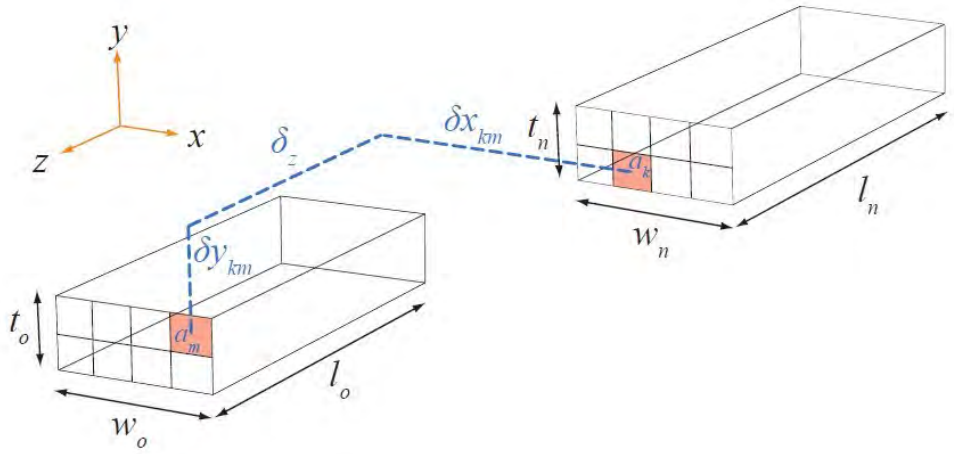

Fig. 2 Layout of variables for mutual partial inductance between two parallel current bars in three dimensions. This treatment further discretizes the bars so that each sub-bar can be treated as a single filament. Each sub-bar in this figure is shaded pink.

The variables δx_{km} and δy_{km} designate the differences in the transverse filament coordinates. Mutual partial inductance is assumed to be zero between bars whose current flow is orthogonal. For differently oriented bars and current flows the calculation simply requires a rotation of the coordinate system.

3.2 Partial capacitance

Capacitive, or electric, coupling is calculated via partial potentials, not partial capacitances. For two conducting bodies, the potential on each one is calculated as

$$\Phi_1 = pp_{11} Q_1 + pp_{12} Q_2 \tag{4a}$$
$$\Phi_2 = pp_{21} Q_1 + pp_{22} Q_2 \tag{4b}$$

where pp_{xx} is the self partial potential and pp_{xy} is the mutual partial potential and $x = \{1, 2\}$, $y = \{1, 2\}$. The partial mutual potential quantifies the potential of an uncharged conductor in the presence of a separate, charged conductor. This relationship, $\Phi_1 = pp_{12} Q_2$, is readily linked to the capacitance between the two conductors, which is $C = Q/V = 1/pp_{12}$, where in this case

$V = \Phi_1 - \Phi_2$, and Φ_2 is considered a common reference potential. Partial potentials thereby quantify the electric or capacitive coupling between conducting patches. The self and mutual partial potentials are, again, calculated separately. Referring to Fig. 3, self partial potentials in free-space are

$$pp_{oo} \approx \frac{1}{6\pi\epsilon\epsilon_0 l_o}\left\{3\ln\left[u+\sqrt{u^2+1}\right]+u^2+\frac{1}{u}+3u\ln\left[\frac{1}{u}+\sqrt{\frac{1}{u^2}+1}\right]-\frac{1}{u}\left(u^2+1\right)^{\frac{3}{2}}\right\}. \tag{5}$$

where u retains its previous definition but now refers to Fig. 3, ϵ_0 is the permittivity of free space, and ϵ is the effective relative permittivity of the surrounding dielectric. Though not discussed here, additional complexity is introduced for metafilms at the boundary between two different media.

Again referring to Fig. 3, the mutual partial potentials are calculated as follows

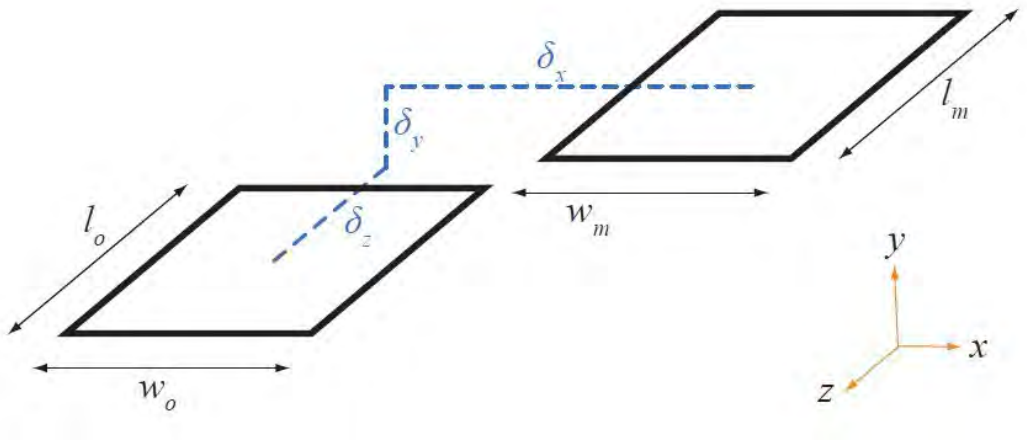

Fig. 3 Layout of integration variables for self partial potential or mutual partial potential between two parallel surfaces.

$$pp_{om} \approx \frac{1}{4\pi\epsilon_0}\frac{1}{w_o u_o u_m v_m}\sum_{i=1}^{4}\sum_{j=1}^{4}(-1)^{i+j}\left[\frac{b_j^2-C_y^2}{2}a_i\ln(a_i+\rho)\right. \tag{6}$$
$$\left.+\frac{a_i^2-C_y^2}{2}b_j\ln(b_j+\rho)-\frac{1}{6}(b_j^2-2C_y^2+a_i^2)\rho-a_i b_j C_y\tan^{-1}\left(\frac{a_i b_j}{\rho C_y}\right)\right]$$

where $C_x = \delta_x/w_o$, $C_y = \delta_y/w_o$, $C_z = \delta_z/w_o$, and $\rho = \sqrt{a_i^2 + b_j^2 + C_y^2}$, and

$$u_o = l_o/w_o$$
$$u_m = l_m/w_o$$
$$v_m = w_m/w_o$$

$$a_1 = C_x - \frac{1}{2} - \frac{v_m}{2}, \qquad a_2 = C_x + \frac{1}{2} - \frac{v_m}{2}$$
$$a_3 = C_x + \frac{1}{2} + \frac{v_m}{2}, \qquad a_4 = C_x - \frac{1}{2} + \frac{v_m}{2}$$
$$b_1 = C_z - \frac{u_o}{2} - \frac{u_m}{2}, \qquad b_2 = C_z + \frac{u_o}{2} - \frac{u_m}{2}$$
$$b_3 = C_z + \frac{u_o}{2} + \frac{u_m}{2}, \qquad b_4 = C_z - \frac{u_o}{2} + \frac{u_m}{2}$$

4. Case studies

Two case studies involving coupled terahertz resonators are convenient for analysis and comparison to previous work. These are comprised of two separate resonators that are closely located to each other such that mutual electric and/or magnetic coupling between the resonators has a significant effect on the overall metamaterial resonance.

4.1 Laterally paired SRRs

The first study is a pair of co-planar SRRs whose gaps face each other, as in Fig. 4(a). The SRRs are otherwise identical, square, and each having an extent of 36 μm. The gap is 4 μm and the lines are 6 μm wide by 200 nm thick. The two SRRs are spaced by 6 μm. As shown in the figure, the SRRs are subdivided into a total of 40 patches, most of which are 6 μm square. Four patches near the SRR gaps are 6 μm × 4 μm. The partial self and mutual potentials were calculated for each and every patch to determine the overall strength of electric coupling between two rings. Figure 5 shows the results of a series of calculations.

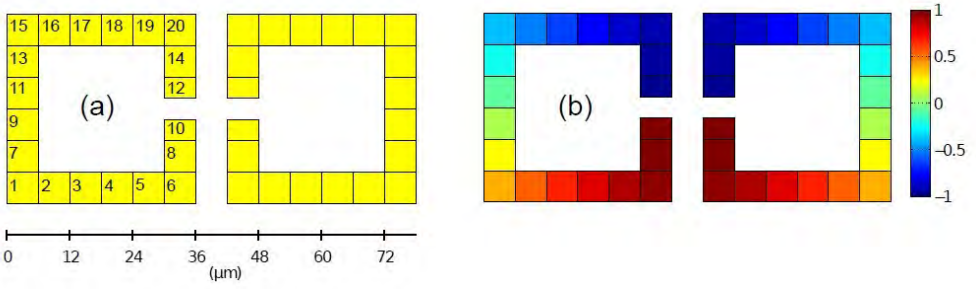

Fig. 4 (a) Laterally-paired SRRs showing patch discretization. Number designators for each patch are displayed on the left SRR. (b) The assumed charge distribution for both SRRs oscillating on the fundamental mode.

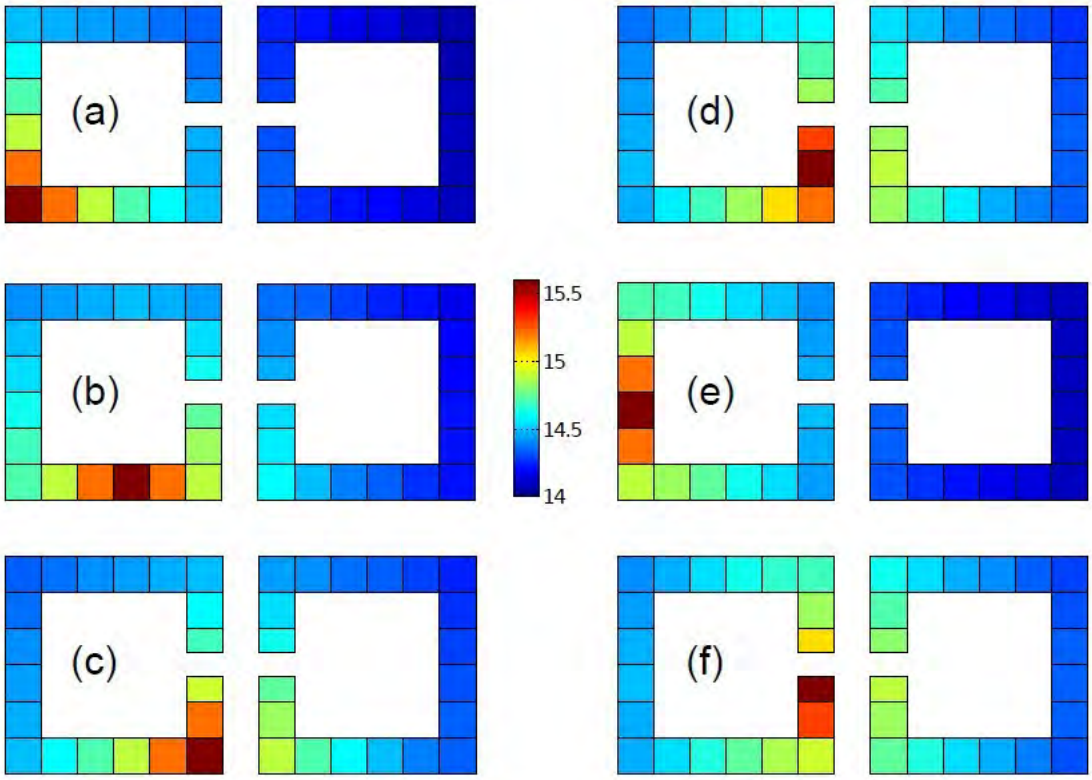

Fig. 5 Self- and mutual- partial potentials between patches of laterally-paired SRRs. For better visualization, the colors show partial potentials on a $\log_{10}$ scale so that a potential of 15 is 10 times stronger than a potential of 14, for example. Calculations are shown for (a) patch 1, (b) patch 4, (c) patch 6, (d) patch 8, (e) patch 9, and (f) patch 10.

Figure 5(a) shows all of the calculated partial potentials to patch number 1. Self-potential is obviously strongest and is therefore colored dark red. All the other patches in Fig. 5(a) are colored according to their mutual potentials to patch 1. Figs. 5(b)-(f) show self- and mutual-potentials to other single patches. In each case, the cell for which all the potentials are calculated is dark red, indicating a strong self-partial potential.

By understanding that these potentials essentially quantify "coupling strength", several conclusions may be reached. First, electric coupling loses most of its strength within a relatively short range, falling to about 1/10 the self-coupling value over a length of only about half the ring width. This suggests that paired SRRs spaced apart from each other as little as half a ring width should experience weak electric coupling and behave largely independently. This also suggests that even within a single ring, most of the distributed capacitive effects arise from interactions between nearby neighboring patches. Finally, for closely spaced patches in paired SRRs, coupling is almost as significant between patches in separate rings as it is for neighboring patches of the same ring. As such, we may expect that electric coupling between the two SRRs will have a significant effect on the resonance in these laterally coupled SRRs.

While these calculations show what coupling is possible, they don't reveal what coupling will

actually occur. To illustrate, two uncharged conductors at zero potential may have a calculable capacitance between them, but they cannot affect each other unless one or the other acquires a nonzero charge. That is, strong coupling does not necessarily imply strong *interaction*. For the paired SRRs, the oscillation mode is necessary to estimate the actual electric interaction strength. Assuming the SRRs are oscillating on the fundamental mode, their charge distribution can be roughly modeled by assuming a circumferential profile of $Q(\theta) \approx \pm \cos(\theta/2)$, where $\theta = [0, 2\pi]$ is an angle measured from the gap bisector about a point in the center of each SRR. This charge distribution is shown in Fig. 4(b).

Incorporating this charge distribution into the partial coupling calculations reveals new figures (Fig. 6) that demon-strate where coupling is significant. Here, interaction strength is calculated by multiplying the partial potential by the patch charge assumed from the mode. Thus, positively (negatively) charged sites produce positive (negative) 'interaction strengths'. Unlike Fig. 5 the colors on these pictures are not logarithmically scaled. Interaction is strongest when both coupling and patch charge are significant, such as for patches near the gap. For the same reason, patches on the vertical sides opposite the gaps have almost no effect whatsoever, such as Fig. 6(d).

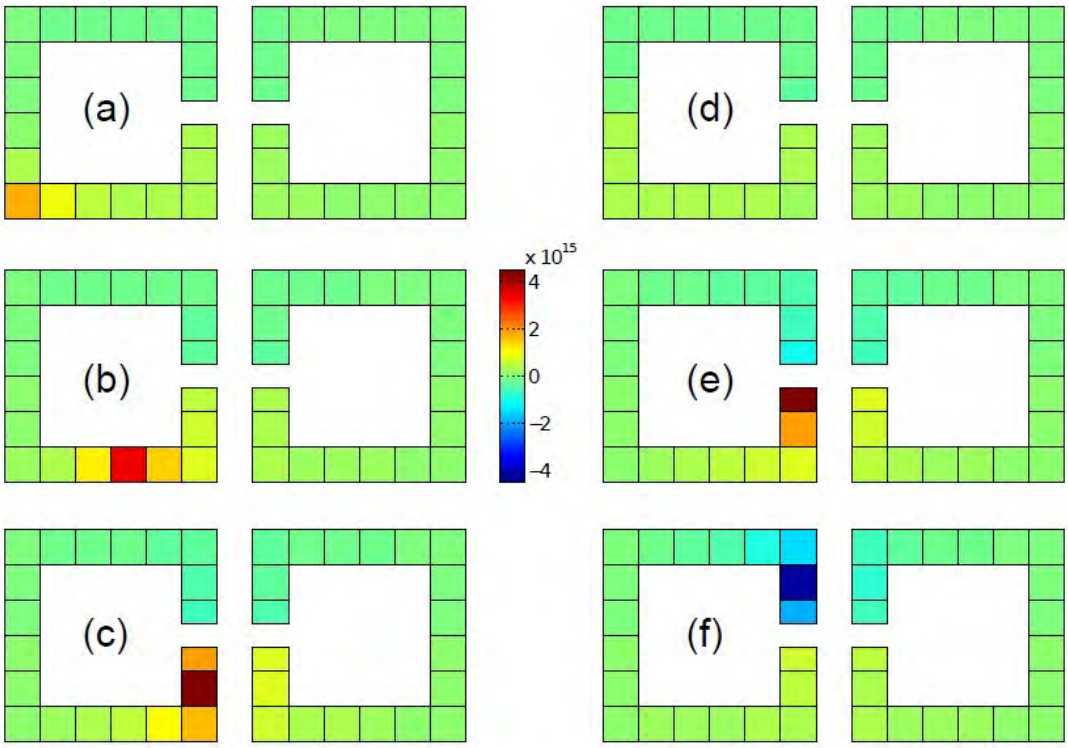

Fig. 6 Interaction strength between patches obtained by multiplying the calculated coupling strength by the patch charge of the fundamental mode. Pictures show interaction strengths between all other patches and: (a) patch 1, (b) patch 4, (c) patch 8, (d) patch 9, (e) patch 10, (f) patch 14. Units of colorscale are C/F, where charge has been normalized between ±1. This reveals that partial potentials have valeus on the order of 2×10^{15} 1/F.

The plots reveal new conclusions. The fundamental mode charge distribution indicates that electric coupling between the two SRRs of a pair will be heavily dominated by interactions near the gaps. On a larger scale, the formation of *arrays* of these ring pairs would have signficant impact on the net metamaterial response. Left or right neighboring pairs will have very little affect on each other. But neighbors above or below could have relatively strong electric coupling effects as the pairs drew close. In this case the SRR corners above and below the gap-bearing arm would strongly interact. Even this coupling could almost eliminated by shifting every other row of pairs horizontally such that gap-bearing arms of one row aligned vertically with non-gap-bearing arms of the neighboring rows. In such a case, strongly charged patches would be situated near weakly charged patches, thereby lessening the effect. The laterally-coupled SRR-pair design, therefore, has variable electric coupling in the vertical direction and little pair-to-pair coupling horizontally.

The magnetic coupling is calculated using the discretization shown in Fig. 7(a). Figure 7(b) shows the current distribution approximation obtained by assuming the SRRs are oscillating on the fundamental mode. Similar to the charge distribution, this is obtained by a simple equation, $I(\theta) \approx \pm \sin(\theta/2)$, where $\theta = [0, 2\pi]$, is the angle measured from the gap bisector around a point in the center of each SRR. Interaction strength is again determined by two factors. Here they are the coupling strength and the magnitude of current flow in the bars. Combining these produces a picture, in Fig. 8 of the interaction strength of each individual bar with all the other bars in the paired-SRR structure.

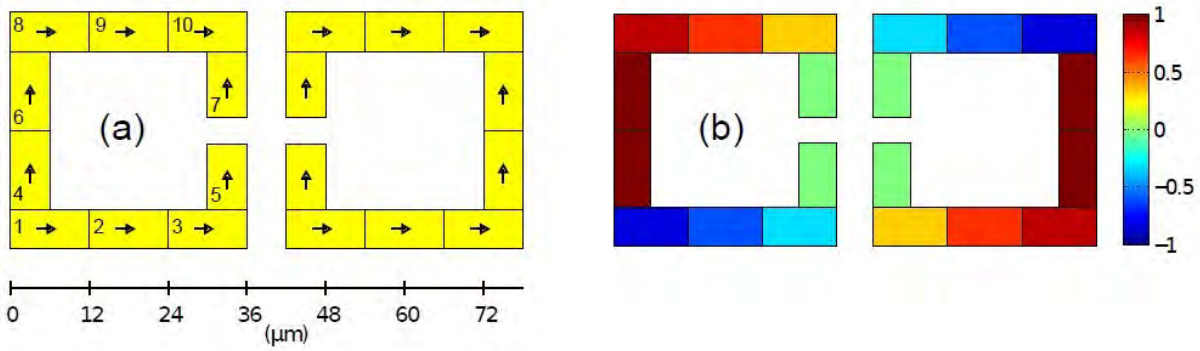

Fig. 7 (a) Discretization of horizontally- and vertically- directed current bars. (b) assumed current in each bar, where a negative value indicates current flows in the direction opposite the arrow in (a). Number designators for each bar are displayed on the left SRR.

From these plots several conclusions may be drawn. First, there is very little magnetic interaction between the paired rings around their gaps. The *coupling* strength between vertical bars surrounding the gap is actually strong, but since very little current flows, it is of no consequence. Current flow is strongest in the vertical bars opposite the gaps, but like the electric interactions, coupling has a short range. Consequently, the overall magnetic interaction between the paired SRRs is low. Much more significant magnetic coupling should be expected in arrays of pairs, however, in both the vertical and horizontal directions, as long as the pairs are packed

densely in the array. In a rectangular array of these pairs, for example, the non-gap-bearing sides of the SRRs form separate pairs would interact strongly due to close range and high currents.

4.2 Bilayer opposing SRRs

In the second case study, the unit cell is comprised of two paired SRRs, separated 6 μm in the direction of terahertz propagation and whose gaps face opposite directions, as shown in Fig. 9. Only the current cells are shown. The charge distribution in each SRR is assumed to be the same as in Fig. 4(b).

Since charge accumulation is very low in the non-gapped vertical arms, the electric interaction strength between SRRs in this pair appears to be dominated by coupling along the top and bottom horizontal sides of the SRRs, as shown in Fig. 10. Based on the assumed mode, the charges in both SRRs are of equal sign where their interaction is significant. With small enough spacing between SRRs, and with the symmetry of the system, the consequent repulsive, electric interaction at the top and bottom of this ring may be expected to blue-shift the overall resonance and set up a dipolar-like mode in the structure as a whole. Indeed, such a phenomenon has been observed; this structure is known to operate as a single closed ring with a dipolar-type oscillation mode [7] as the spacing between rings approaches zero.

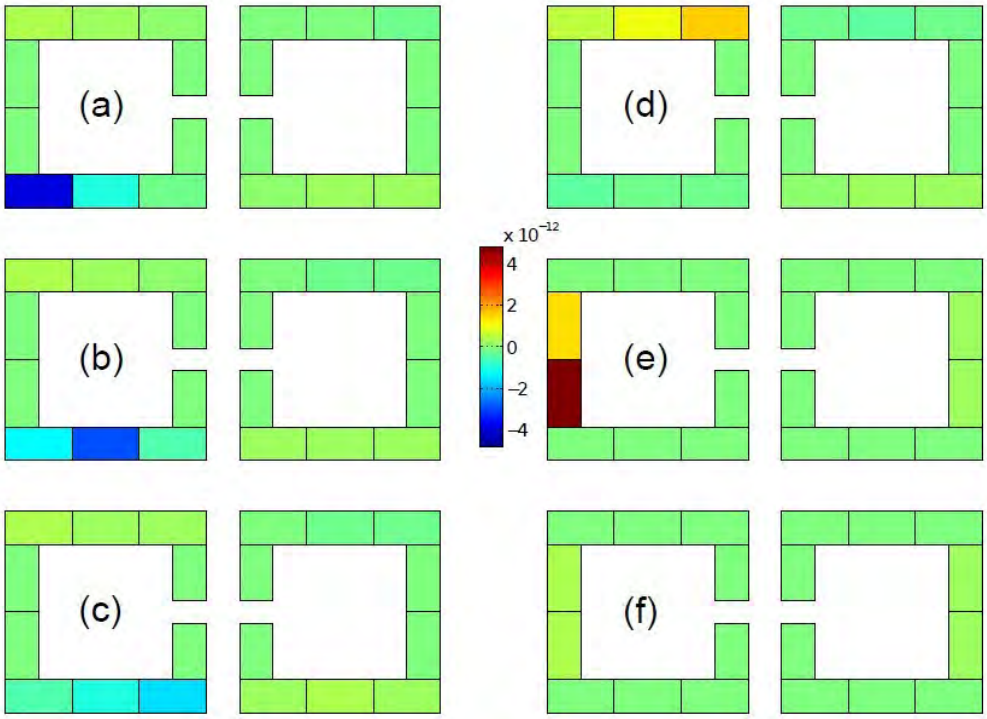

Fig. 8 Interaction strength between bars obtained by multiplying the calculated coupling strength by the magnitude of current flow in other bars. Colors show interaction strengths of all the bars, calculated for: (a) patch 1, (b) patch 2, (c) patch 3, (d) patch 10, (e) patch 4, (f) patch 5. Negative strengths simply indicate currents flowing in opposite directions. Units of colorscale are A-H, where current has been normalized between ±1. This reveals the partial inductances have values on the order of 2×10^{-12} H.

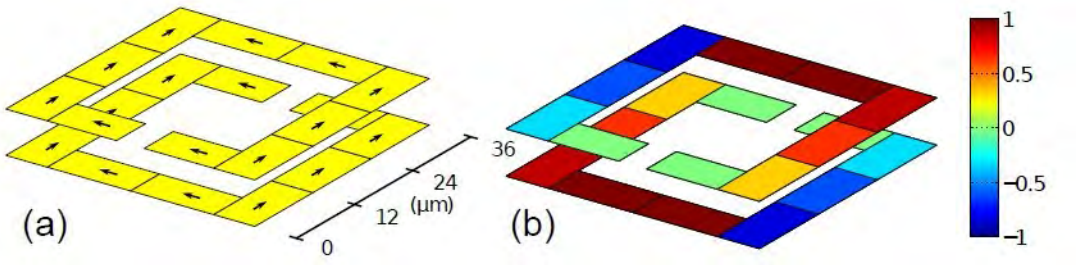

Fig. 9 (a) Bilayer paired SRRs with opposing orientation. Arrows indicate assumed direction of current flow for coupling calculation. (b) Fundamental mode current distribution, where sign of current is commensurate with arrow designators in (a). "Horizontal" arms of the SRRs are those orthogonal to the gap-bearing arms.

The magnetic coupling is also dominated by the horizontal arms of the SRRs, as shown in Fig. 11. Assuming the fundamental mode as in Fig. 9(b), the magnetic interaction should cause a blue-shift to the overall metamaterial resonance as the layers become closer. This is indicated by the opposing sign of the current flows in the horizontal arms of the SRRs in Fig. 11. Thus, both the electric and magnetic effects should blue-shift the resonance.

4.3 Bilayer opposing SRRs reversed mode

The final case study is exactly the same as the last, except the current mode of the upper ring is reversed in direction. The resulting charge and current profiles were calculated as usual with the exception of changing their sign in the 9 upper SRR. These modes are shown in Fig. 12. The resulting calculations are very similar to those of the original bilayer structure and are shown in Fig. 13.

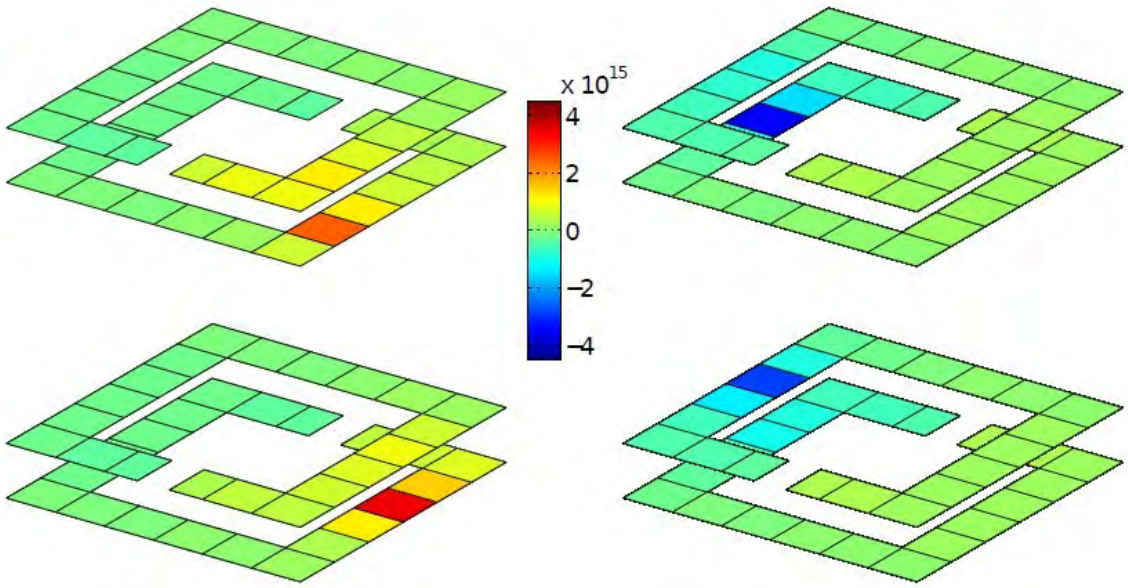

Fig. 10 Dominant electric interactions in the opposed-gap bilayer SRR pair. Interactions along the vertical (gap-bearing and opposite) arms are limited by weak charge accumulation in one or the other SRR.

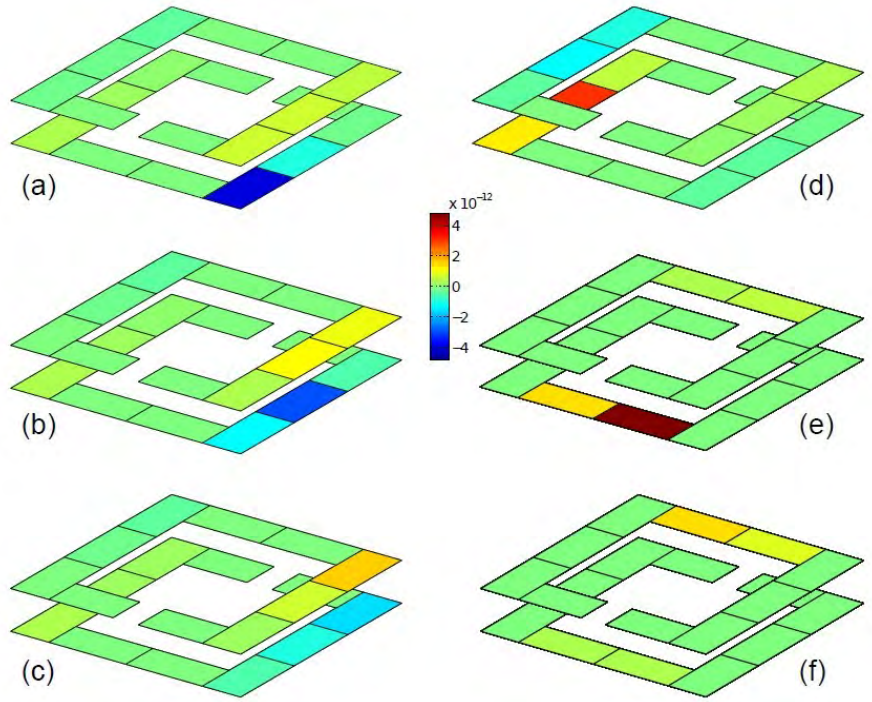

Fig. 11 Dominant magnetic interactions in the opposed-gap bilayer SRR pair occur in the horizontal arms of the SRRs (a)-(d). Interactions along the vertical (gap-bearing and opposite) arms, (e) and (f), are limited by weak currents that flow near the gaps of the SRRs.

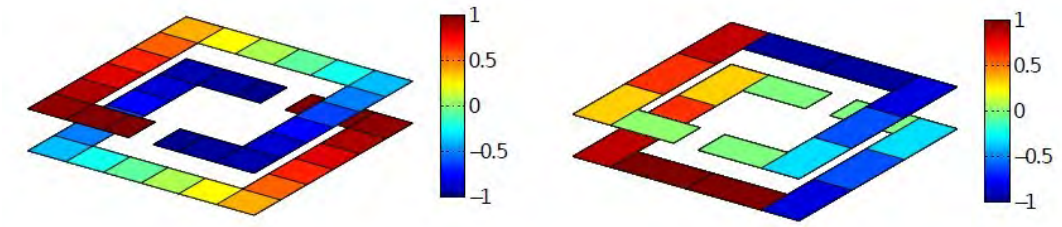

Fig. 12 Reversed upper SRR mode bilayer structure assumed charge and current distributions.

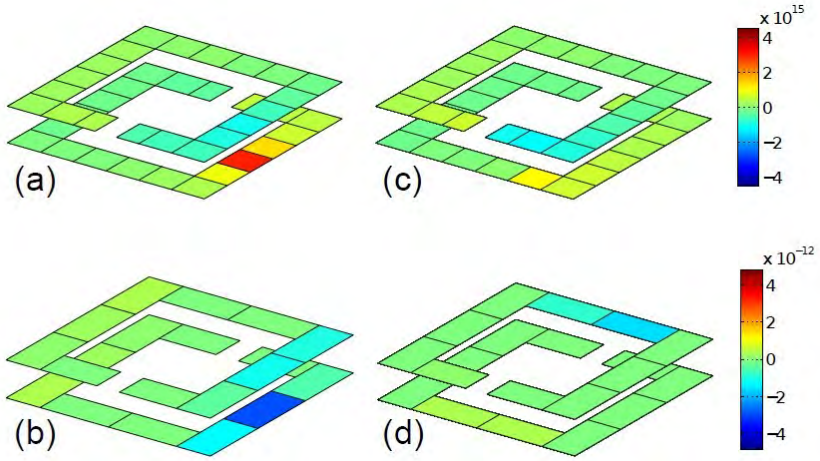

Fig. 13 Dominant interactions in reversed mode bilayer structure (a) relatively strong electric interaction in lower, horizontal SRR arms, (b) relatively strong magnetic interaction in lower, horizontal SRR arms, (c) weak electric interaction near left gap, (d) weak magnetic interaction near right gap.

The calculations suggest that both electric and magnetic interactions are again dominated by the horizontal arms of the SRRs. Since the coupling calculations have not changed at all, the only change in the interaction is due to the assumed modes. This is an important change, however, since the electric and magnetic interactions are now oriented in sign such that they both contribute to a red-shift in the resonance as the SRR spacing is reduced. This result is also consistent with previous terahertz metamaterial work involving this type of structure and mode [7].

5. Discussion

5.1 Estimating frequency shifts

In the discussions above, mention was made several times regarding the expected frequency shift of the resonance as the paired SRRs were drawn closer to each other. In general it is not always obvious how the resonance will be affected in paired SRRs, based only on a visual picture of the interactions. An example would be a bilayer SRR structure in which the gaps are aligned. Such a structure would have very strong electric and magnetic coupling around the entire SRR circumference. And, if the modes were equally 'aligned', a tremendous blue shift in the resonance might be expected due to the electric interaction, while a tremendous red shift might be expected due to the magnetic interaction. However, virtually no change at all is actually observed in the resonance. It is therefore important to quantitatively estimate resonance shifts. Since this analysis method is quantitative, such a task is possible. We defer the details to later work, however the general idea is to sum the total electric and magnetic interaction contributions for each and every patch and bar. The same procedure is applied to a single, unpaired SRR. Ratios' are formed from the magnetic and electric interactions derived from the single and paired SRRs. If the ratio of magnetic interactions matches that of the electric interactions, it is expected that little to no shift will be observed by pairing the structures. This is the case for the aligned bilayer structure, for example. If the ratio of magnetic interactions is unequal to the electric interaction ratio, then one or the other is dominating and the resonance will shift accordingly. A few further details remain to be derived in this 'ratio' method to fully quantify the expected shift, suffice to say it is possible.

5.2 Analysis limitations

The partial calculations presented above are electrostatic and magnetostatic in nature, therefore time-retardation is ignored. Of course, retardation is fully expected in an oscillating system, and the principle effect of this omission is the elimination of radiation mechanisms. Time-delays cause an imaginary term to enter the coupling coefficients thereby introducing loss. Since this is not Ohmic loss, it is quickly realized this is the exact mechanism of radiation. Similarly, skin effects are ignored. For thick conductors at high frequency, some account should be made of the inhomogeneous current profile in the discretized bars. While these ommissions reduce the

accuracy of this method, they remain largely consistent with a lumped-circuit approximation of the metamaterial resonator, and the structure of most terahertz metafilms. Inaccuracies can certainly be expected in larger resonator systems, such as two coupled resonators, where the overall extent of the system approaches $\lambda/2$.

5.3 Generalizations

The structures analyzed above were chosen to validate the method against previous experimental results [6, 7]. In all cases, the behavior predicted by the coupling analysis matched that of the experimental work. However it was important to choose the proper oscillation mode for the SRRs. These were just assumed for this work, which is often accurate enough. The actual oscillation modes, however, can also be calculated by expanding this coupling analysis into what's known as the Partial Element Equivalent Circuit (PEEC) method [18]. Here, the movement of charge around the structure is linked to the calculated currents and potentials at each node forming a integrated system involving both the electric and magnetic coupling calculations. Neglecting time-retardation, modal analysis is then performed on this linked system and will reveal the time-harmonic current and charge distributions around the SRRs. This amounts to a simplified Moment Method type full-wave simulation. Figure 14 shows the two lowest order modes of the opposed-gap bilayer structure calculated from this method.

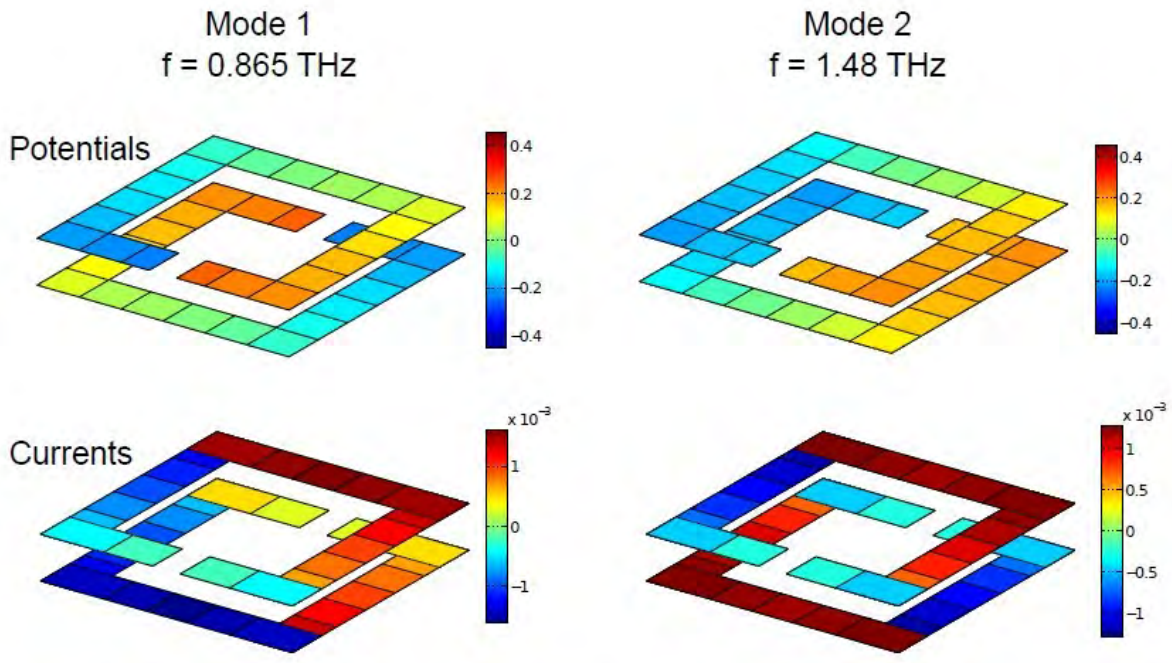

Fig. 14 Potential and current mode maps produced for the opposed-gap bilayer structure using Partial Element Equivalent Circuit analysis and coupling calculations above. Potential maps are at the top and current maps at the bottom. Mode 1 is on the left, and mode 2 is on the right. Additional current bars had to be added to enable this calculation. Currents are scaled in color according to the direction convention in Fig. 9(a).

It is apparent that the original assumptions about the form of the modes, used in the partial potential and inductance calculations, were fairly accurate. The PEEC modal analysis also provides the expected resonance position of each mode fairly accurately, when compared to full-wave simulations using commercial electromagnetic solvers. Suffice to say, the direction of resonance shift can be readily calculated by this modal analysis, with generality above that of the 'ratios' method described above. Since the goal of this work was only to introduce the coupling analysis, such details will be deferred to a later manuscript.

5.4 Applications

As stated earlier, numerous terahertz studies have focused on coupling between resonator elements in the metamaterial. And these studies have provided new methods of tuning the macroscopic metamaterial response. As an example, the reversed-mode bilayer structure is readily expected to exhibit a strong red-shift in the macroscopic resonance. As such, this is an obviously good candidate unit cell for creating a resonator whose spatial extent is much smaller than the operating wavelength. Indeed, this was discussed in our previous work [7]. The coupling analysis presented above will be useful for quickly testing and designing coupled terahertz metamaterials with some desired behavior. The calculations performed above may be completed in less than one second. Furthermore, coupling may be turned on or off at any bar or patch to determine and isolate the effects on the macroscopic resonance.

Even more interest has recently been directed toward propagating waves that might exist on a terahertz metafilm surface. The so-called magneto- or electro-inductive waves rely on energy moving from SRR-to-SRR through the magnetic or electric coupling mechanism [19–21]. Recent work involves the study of arrays of coupled, nonlinear, SRRs [22]. Myriad fascinating electromagnetic phenomena occur in such system, including soliton generation, wave mixing, and quasi-chaotic oscillations. Many of these *require* some amount of interaction strength between neighboring SRRs. Most available full-wave simulators cannot easily handle the nonlinearities involved in such systems. Our coupling analysis, however, is relatively simple, and readily links metamaterial behavior to simple *RLC* lumpedcircuit concepts. Yet it offers sufficient accuracy to provide realistic estimations of metamaterial behavior. As such it permits rapid study of nonlinear, coupled-SRR metamaterial phenomena, which is certainly a strong, upcoming research direction in terahertz metamaterials.

6. Conclusion

We have presented an analytical method for quanitatively estimating the coupling and interaction strength in resonators comprising terahertz metamaterials. This method, borrowed from the electromagnetic compatibility arena, quickly provides a visual picture of where SRRs or other resonator components are strongly coupled to neighbors, both electrically and magnetically. The analysis also provides quantiative estimates of resonance shifts and overall interaction

strengths suitable for creating relatively simply lumped-circuit models of terahertz metamaterials. These can assist the researcher in quickly designing a required metamaterial response and provide intuitive insight where full-wave methods are lacking. Furthermore, the simplicity of this method lends itself to numerous advanced studies in nonlinear terahertz metamaterials.

Acknowledgments

The authors gratefully acknowledge support from Los Alamos National Laboratory Grant LDRD 20110027DR.

References

[1] W. Padilla, A. J. Taylor, C. Highstrete, et. al. *Phys. Rev. Lett* 96, 4 (2006).

[2] H.-T. Chen, W. J. Padilla, J. M. O. Zide, et. al. *Nature* 444, 597–600 (2006).

[3] H.-T. Chen, J. F. O'Hara. . . , A. K. Azad, et. al. *Nature Photon* 2, 295–298 (2008).

[4] A. K. Azad, A. J. Taylor, E. Smirnova, et. al. *Appl. Phys. Lett* 92, 011119 (2008).

[5] D. R. Chowdhury, R. Singh, M. T. Reiten, et. al. *Optics Express* 19, 15817–15823 (2011).

[6] D. Chowdhury, R. Singh, M. T. Reiten, et. al. *Optics Express* 19, 10679–10685 (2011).

[7] M. T. Reiten, D. R. Chowdhury, J. Zhou, et. al. *Appl. Phys. Lett* 98, 131105 (2011).

[8] J. Gu, R. Singh, X. Liu, et. al. *Nature Communications* (2012).

[9] R. Singh, C. Rockstuhl, F. Lederer, et. al. *Phys. Rev*. B 79, 4 (2009).

[10] D. R. Chowdhury, R. Singh, A. J. Taylor, et. al. *International Journal of Optics* 2012, 1–12 (2012).

[11] J. Zhou, H. Chen, T. Koschny, et. al. *arXiv* 1111.0343, 1–5 (2011).

[12] H. Chen, J. Zhou, J. F. O'Hara, et. al. *Phys. Rev. Lett* 105, 73901 (2010).

[13] J. Zhou, D. R. Chowdhury, R. Zhao, et. al. *Physical Review* B 86, 35448 (2012).

[14] D. R. Chowdhury, R. Singh, A. J. Taylor, et. al. *Applied Physics Letters* (2013).

[15] A. E. Ruehli, *IBM J. Res. Develop* 16, 470–481 (1972).

[16] A. E. Ruehli, P. A. Brennan, *IEEE transactions on microwave theory and techniques* 21, 76–82 (1973).

[17] J. F. O'Hara, E. Smirnova, A. K. Azad, et. al. *Active and Passive Electronic Components* 2007, 1–11 (2007).

[18] A. E. Ruehli, *IEEE transactions on microwave theory and techniques* 22, 216–221 (1974).

[19] N. Liu, S. Kaiser, H. Giessen, *Adv. Mater* (2008).

[20] O. Sydoruk, E. Shamonina, L. Solymar, *Journal of Physics D: Applied Physics* 40, 6879–6887 (2007).

[21] E. Shamonina, *Physical Review* B 85, 155146–1–4 (2012).

[22] P. L. Colestock, M. T. Reiten, J. O'Hara, *Metamaterials* 1–19 (2012).